# Bi-layer stiffness identification of soft tissues by aspiration

N Connesson, N Briot, P Y Rohan, P A Barraud, S A Elahi, Y Payan

**Noname manuscript No.**
(will be inserted by the editor)

# Bi-layer stiffness identification of soft tissues by aspiration.

**N. Connesson · N. Briot · P.Y. Rohan · P.A. Barraud · S.A. Elahi · Y. Payan**

Received: 08/07/2022 / Accepted: date

**Abstract** The aim of this work was to develop both experimental and inverse analyses methods of aspiration/suction measurement onto bilayered soft tissues structures.

An original aspiration system is described. The main features are volumic measurements (no camera or mirror constraining the aperture design), cyclic partial vacuum (reproducibility, airtightness checking), low deformation loading (elasticity domain, damageless for *in vivo* and *in situ* applications) and the use of disposable aspiration cups of various aperture diameters ranging between 4 and 30 mm (easy to sterilize, adaptable to accessibility constaints).

The aspiration system was tested *in silico* on controlled silicone bilayer specimens (reference layers' Young Moduli characterized by tensile test, reference layers' thickness destructively measured *a posteriori*); the apparent stiffness of the bilayer structure is measured for 9 different aperture sizes.

Using the experimental apparent stiffness changes with diameters, (i) the upper and lower layer Young moduli are identified in almost real-time using

Corresponding Author
TIMC-IMAG Laboratory, UMR CNRS 5525, Grenoble Alpes University, Pavillon Taillefer, Faculty of Medicine, Domaine de la Merci, 38706 La Tronche cedex, France.
E-mail: nathanael.connesson@univ-grenoble-alpes.fr

a Finite Element database interpolated with a Principle Component Analysis. Optionally, the optimal upper layer thickness is also identified. (ii) the possible ill-posedness of the problem is analysed in terms of parameter identifiability/indifference region (prediction of experimental standard deviation).

For an upper layer thickness of about 3 *mm*, the Young moduli identified by aspiration onto a bilayer sample presented a relative error lower than 10% compared to reference values. The layer thickness was also identified with an error lower than 2%.

These validations give confidence to apply this method *in vivo* and *in situ* to soft tissues such as human skin if considered as bilayered structures.

**Keywords** Suction/Aspiration Method · Soft tissues Characterization · in vivo Measurement · Validation on silicone specimens · Inverse Finite Element Analysis · Experimental Mechanics.

## 1 Introduction

Since the pioneer book of Yuan-Cheng Fung published in 1981 [1], many research groups in the world have designed biomechanical models of human soft tissues for applications such as Computer Assisted Medical Interventions [2]. To be relevant, these computational models must be adapted in terms of geometrical and mechanical behavior which are unfortunately subject-specific, age dependent and which can differ significantly between *in vivo* and *ex vivo* conditions (*e.g.* vascularization of the tissue [3–5], preservation process [6], *etc*). Moreover, biological tissues usually exhibit nonlinear, time dependent, inhomogeneous, and anisotropic behaviors. It is also well-known nowadays that such tissues develop, grow, remodel, and adapt so as to maintain particular mechanical target metrics (*e.g.*, stress).

In practice, the diversity of encountered phenomena for soft tissue modeling is simplified by choosing constitutive models and parameter identification methods. As such, most complex nonlinear stress-strain curves of human soft tissues can be identified *ex vivo* through experimental tests such as uni or bi-axial tensile tests [6–9], pure shear [9, 10], plain strain compression [9], bulge tests [11, 12], indentation [13, 14] or aspiration [15]. If such tests proved invaluable, they can usually not simply be performed *in vivo*.

These observations higlight the extensive work to be dealt with for *in vivo* characterization. A first step toward this direction is the estimation of subject-specific tissue stiffness, which is even in itself a challenge. This property is usually the prerequisite to clinical use of any model in the context of Computer Assisted Medical Interventions.

A possibility largely studied method is to use aspiration techniques [16], consisting in putting a sterile chamber with an aperture in contact with the investigated tissue and in decreasing the pressure inside the chamber. The amount of tissue aspirated is related to tissue stiffness. The aspirated tissue height is generally estimated either using ultrasound methods [17, 18], mechanical stops [19], optical coherence tomography [18] or cameras usually associated with mirrors or prisms [20–28].

To widen the use of such method, it would make sense to design the system so that the head is unexpensive, disposable, highly customizable (aperture size, shape, material) and able to meet any required severe sterilization process. Our group has thus recently proposed to replace the measurement of the tissue height with the measurement of the aspirated tissue volume [29]. Such a change in the method enables the elimination of camera, mirror, prism, and all the electronic parts from the system head that was basically reduced to a simple tube with an aperture. The corresponding device, called VLASTIC, enable to evaluate silicones stiffnesses with a maximal error of about 10% compared to

uniaxial tensile tests [30]. It was also used in a clinical study to evaluate the tongue stiffness in ten patients for two conditions: at rest and under general anesthesia [31]. Yet, in these studies, the underlying tissues were assumed homogeneous. As most human tissues are inhomogeneous, the method must be further developed.

The homogeneity hypothesis while using aspiration was challenged in literature. When extracting only the superficial layer mechanical properties, Zhao *et al.* [15] demonstrated *in silico* that an aspiration diameter smaller or equal to the upper layer thickness should be used. Other works [25, 32, 33] use data from tests with two different diameters (2 and 8 mm) to estimate the mechanical response of the most superficial layers of the human skin, and sometimes complete the data using *ex vivo* tensile test [33]. In [18], 3 diameters (1, 2 and 6 mm) and Optical Coherence Tomography were used to evaluate the mechanical behavior of the softer 130 $\mu m$ upper skin layer.

This work aims at going beyond the state of the art (i) by using a single, easy to use and adaptable aspiration system, switching only aperture heads to perform all the measurements, (ii) by proposing identification of Young moduli of each constituent of bi-layered structures using an off-line Finite Element database (almost real time identification), (iii) by evaluating the parameter identifiability of the tested situation

The whole method has been evaluated experimentally to test the ability of VLASTIC to estimate the stiffnesses of bi-layers silicone phantoms compared with classical experimental tensile tests.

To the author's knowledge, no previous work implemented these last points. The hope is that the VLASTIC system and method will be used to estimate mechanical properties of most accessible soft tissues, such as for example the skin stiffness for face [34, 35], breast [36], sacrum [37] or foot [38] modeling.

## 2 Material and Methods

As an overwiew, the paper structure is graphically summarized in figure 1.

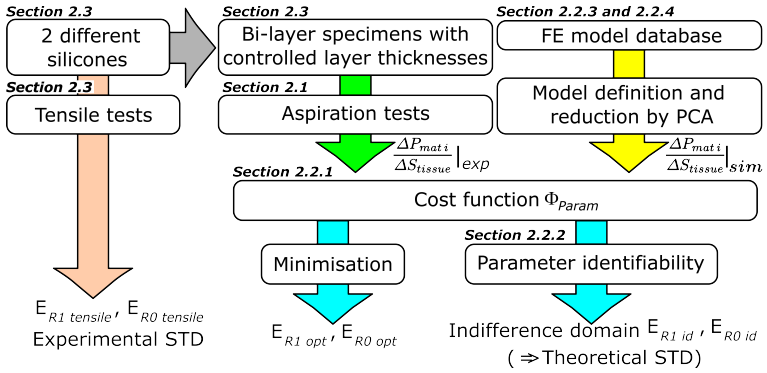


**Fig. 1** Paper structure and main output notations: $E_{R1\,tensile}$ and $E_{R0\,tensile}$ stand for both layers' Young moduli measured through uniaxial tensile test on specimens. $E_{R1\,opt}$ and $E_{R0\,opt}$ are Young moduli identified with aspiration data and minimizing the cost function $\Phi_{Param}$.

### 2.1 Volume based aspiration tests

#### *2.1.1 Cyclic testing device*

The testing system is composed of two air-filled parallel circuits defined as "Reference line" and "Material line", respectively, both connected at a valve, a manometer[a] and a syringe[b] (Figure 2 a). The syringes stroke $\Delta L$ is simultaneous and cyclic, inducing a volume variation $\Delta V$ in each line.

The "Reference line" is simply a tube closed at its end. It converts the volume variation $\Delta V$ (that may not be perfectly controlled during movement inversions due to the syringe piston deformation) into a pressure variation $\Delta P_{ref}$. The tube length is chosen so that the pressure variation $\Delta P_{ref}$ in

[a] AMS-5812-0015-D-B, Analog Microelectronics GmbH
[b] CODAN 1mL Luer TBC

the "Reference line" sweeps the whole sensor pressure range given the input volume variation $\Delta V$.

The "Material line" is composed of a tube linked to a 3D printed resin cup of aspiration diameter $D_i$ (Figure 2 d) applied on the tested tissue. All cup geometrical features in contact with the tested tissue (wall thickness, fillet radius, *etc.*) are proportional to the aperture diameter $D_i$. This line converts the input volume variation $\Delta V$ into a pressure variation $\Delta P_{mat}$.

The general idea is that the tested tissue mechanical behavior can be deduced by comparing the pressures variations in the two lines ($\Delta P_{ref}$ and $\Delta P_{mat}$) while testing the tissue or an undeformable material (calibration test); the ratio of pressure variation in both lines $\frac{\Delta P_{ref}}{\Delta P_{mat}}$ will change between these two cases and contains the sought properties.

### *2.1.2 Protocol and elastic model*

Practically, every test starts with the same protocol:

- ✓ The cup $D_i$ is placed on the tested material. An ultrasound gel cord fills an external groove to ensure air tightness. The syringes are set in their empty reference position using the homing sensor (Figure 2 b). The valves are then closed, the air volume enclosed in the system being thus reproducible and minimum at the starting point ($n = 0$).
- ✓ A volume $\Delta V$ is withdrawn simultaneously and cyclically from both the material and reference lines (Figures 2 a and b). The pressure variations $\left(\Delta P_{ref},\, \Delta P_{mat\,i}\right)_n = \left(P_{ref\,n} - P_{ref\,0},\, P_{mat\,i\,n} - P_{mat\,i\,0}\right)$ are measured in the reference and material lines, respectively. The underscript $n$ represents the pressure index.
- ✓ Pressure variations during the test $\left(\Delta P_{ref},\, \Delta P_{mat\,i}\right)_n$ are supposed proportional to the volume variation $\Delta V$ using elastic stiffnesses in a spring

model (Figure 2 c) such as:

$$k_{ref} = \frac{\Delta P_{ref}}{\Delta V} \tag{1}$$

$$k_{cup\,i} = \frac{\Delta P_{mat\,i}}{\Delta V_{cup\,i}} \tag{2}$$

$$k_{tissue\,i} = \frac{\Delta P_{mat\,i}}{\Delta V_{tissue\,i}} \tag{3}$$

$$\text{where } \Delta V = \Delta V_{tissue\,i} + \Delta V_{cup\,i} \tag{4}$$

To simplify the notations, expressions are articulated in the next equations using the ratio $Q_{i\,X}$ defined as:

$$Q_{i\,X} = \frac{\Delta P_{ref}}{\Delta P_{mat\,i}} \tag{5}$$

where underscript $i$ refers to the aperture diameter $D_i$ and $X$ indicates whether $Q_{i\,X}$ is obtained during a calibration step ($X = cal$) or by testing a tissue ($X = exp$).

In practice, the ratios $Q_{i\,exp}$ and $Q_{i\,cal}$ are slopes of linear poynomial identified on the $\left(\Delta P_{ref},\, \Delta P_{mat\,i}\right)_n$ curve. It can be obtained by minimizing the linear function $\Phi_Q$ defined in the least square sense:

$$\Phi_Q = \sum_{n=1}^{N} \left( \Delta P_{ref} - (Q_{i\,X}\, \Delta P_{mat\,i} + A) \right)_n^2 \tag{6}$$

where $N$ is the number of used pressure measurements and $A$ is a constant accounting for any pressure offset difference between the material and reference lines due to potential thermal drifts.

### *2.1.3 Calibration and measurement*

The system reference and material lines must be calibrated before testing deformable tissues:

- **Calibration of the "Reference line" (stiffness $k_{ref}$):**

  Different cyclic volume amplitudes $\Delta V$ are applied to the reference line by increasing step by step the syringe courses $\Delta L$ with an adjustable 500 $\mu m$ thread pitch screw-driven eccentric mecanism (Figure 2 b). The slope of the pressure variation amplitude $\Delta P_{ref}$ versus the volume amplitude $\Delta V = \Delta L\, S_{syringe}$ is the sought reference line stiffness $k_{ref} = 0.992\ mbar.mm^{-3}$ (equation 1).

- **Calibration of the "Material line" for each cups (ratio $Q_{i\,cal}$):**

  The material line is calibrated for each cup $D_i$ applied on an undeformable material ($k_{tissue} = \infty, \Delta V_{tissue\,i} = 0$). Equation 5 simply provides the material line ratio $Q_{i\,cal}$ during calibration:

$$Q_{i\,cal} = \frac{\Delta P_{ref\,cal}}{\Delta P_{mat\,i\,cal}} \tag{7}$$

- **Test on deformable tissue $k_{tissue\,i}$:**

  When testing a soft tissue, the tissue apparent stiffness $k_{tissue\,i}$ is computed combining equations 1 to 5 and 7 so that:

$$k_{tissue\,i} = \frac{k_{ref}}{Q_{i\,exp} - Q_{i\,cal}} \tag{8}$$

  Note that the information about the tissue apparent stiffness $k_{tissue\,i}$ is mainly contained in a difference of ratios $Q_{i\,X}$ measured during the calibration and the test on a soft tissue while using the same aperture diameter $D_i$ (see Figure 8b in the results section).

*2.1.4 Apparent stiffness normalization*

The tissue apparent stiffness $k_{tissue\,i}$ contains information about the constituent tissue stiffnesses integrated over the loaded material volume beneath the aperture diameter $D_i$ (Figure 3). Unfortunately, even when testing an

homogeneous material, this stiffness $k_{tissue\,i}$ (in $Pa.m^{-3}$) depends on the aspiration aperture size.

To compare the results obtained with different aperture size, the notion of tissue shape $S_{tissue}$ is defined by normalizing the aspirated tissue volume $V_{tissue\,i}$ by the volume of a half sphere $V_{ref\,i}$ of diameter $D_i$ [31][c]:

$$S_{tissue} = \frac{V_{tissue\,i}}{V_{ref\,i}} \tag{9}$$

$$\text{with} \quad V_{ref\,i} = \frac{4}{6}\pi\left(\frac{D_i}{2}\right)^3 \tag{10}$$

A shape $S_{tissue} = 1$ means a volume of half a sphere has been aspirated into the cup.

Using this shape definition and equation 3, it comes:

$$\frac{\Delta P_{mat\,i}}{\Delta S_{tissue}} = V_{ref\,i}\ k_{tissue\,i} \tag{11}$$

where $\frac{\Delta P_{mat\,i}}{\Delta S_{tissue}}$ (in $Pa$) represents the normalized constituent material apparent stiffness:

On a homogeneous specimen, a change of aperture diameter $D_i$ is equivalent to a change of test scale (same shape obtained for the same pressure variation); the constituent material apparent stiffness $\frac{\Delta P_{mat\,i}}{\Delta S_{tissue}}$ is independent of aperture-diameter $D_i$.

On bi-layered specimens, a change of aperture diameter $D_i$ modifies the upper layer relative contribution to the shape $S_{tissue}$ (Figure 3, illustration for $S_{tissue} = 1$). In particular, a cup of diameter smaller or equal to the thickness $L_{R_1}$ of the upper layer of material labeled $R_1$ mainly extracts the upper layer stiffness [15] as will be further developped in section 3.

[c] Similar normalization of the apex hight is also found in [15].

Combining equations 8 and 11, the normalized constituent material apparent stiffness $\frac{\Delta P_{mat\,i}}{\Delta S_{tissue}}$ is thus simply obtained by:

$$\frac{\Delta P_{mat\,i}}{\Delta S_{tissue}} = V_{ref\,i}\ \frac{k_{ref}}{Q_{i\,exp} - Q_{i\,cal}} \tag{12}$$

## 2.2 Bi-layer mechanical properties inverse identification

The inverse identification consists in estimating both layer Young's moduli ($E_{R1}$ and $E_{R0}$), and optionnally, the thickness $L_{R1}$ of the upper layer, minimizing a cost function $\Phi_{Param}$ (section 2.2.1). A Finite Element (FE) model has been created to simulate the aspiration procedure and predict each parameter effect.

### *2.2.1 Cost Function*

The cost function $\Phi_{Param}$ is defined in the least square sense on the experimentaly measured material apparent stiffness $\left.\frac{\Delta P_{mat\,i}}{\Delta S_{tissue}}\right|_{exp}$:

$$\Phi_{Param} = \sum_{i=1}^{I} \frac{1}{\sigma_i^2} \sum_{j=1}^{J_i} \left( \left.\frac{\Delta P_{mat\,i}}{\Delta S_{tissue}}\right|_{sim}(\theta,\beta) - \left.\frac{\Delta P_{mat\,i}}{\Delta S_{tissue}}\right|_{exp} \right)_j^2 \tag{13}$$

where $\left.\frac{\Delta P_{mat\,i}}{\Delta S_{tissue}}\right|_{sim}$ is the simulated material apparent stiffness for a cup diameter $D_i$ (section 2.2.3 and 2.2.4), $\theta$ is a $P$-dimensional vector representing the sought unknowns and referred to as "parameter vector", and $\beta$ represents the other model parameters (aperture diameter, friction, compressibility coefficient, *etc.*). $I$ is the number of aperture diameter $D_i$ used and $J_i$ is the number of cycles performed for each aperture of diameter $D_i$. The number of measurements used to compute $\Phi_{Param}$ is thus $N_m = \sum_{i=1}^{I} J_i$. The weighing denominator $\sigma_i^2$ is the experimental unbiased variance of the experimental apparent stiffness $\left.\frac{\Delta P_{mat\,i}}{\Delta S_{tissue}}\right|_{exp}$ for aperture $D_i$ and is used so that the cost

function $\Phi_{Param}$ is not dominated by the experimental data provided by a specific aperture diameter $D_i$ [39].

Unknowns and model parameters $\theta$ and $\beta$ are composed of four main characteristics (Figure 3), namely the aperture diameter $D_i$, the upper layer thickness $L_{R_1}$ and associated Young's modulus $E_{R1}$ and the lower layer Young's modulus $E_{R0}$. The optimal parameter vector $\theta_{opt}$ minimizing the cost function $\Phi_{Param}$ is estimated using the Levenberg-Marquardt method [40] under different situations referred to by the number of sought parameters $P$.

$P = 3$ **(bi-layer,** $\theta =< E_{R1}, E_{R0}, L_{R_1} >^T$**:** when the specimen is a bi-layer specimen, the upper layer thickness $L_{R_1}$, Young's modulus $E_{R1}$ and the lower layer Young's modulus $E_{R0}$ can all be estimated.

$P = 2$ **(bi-layer,** $\theta =< E_{R1}, E_{R0} >^T$**):** when the specimen is a bi-layer specimen, the upper layer thickness shall be provided in $\beta$ by an annex measurement. In such a case, only the upper and lower layer Young's moduli $E_{R1}$ and $E_{R0}$ are estimated in $\theta$.

$P = 1$ **(homogeneous,** $\theta =< E_{R1} >$**):** when the specimen is considered homogeneous, only the averaged material Young's modulus is estimated ($E_{R1} = E_{R0}$). In such a case, the theoretical constituent material apparent stiffness $\frac{\Delta P_{mat\,i}}{\Delta S_{tissue}}\big|_{sim}(\theta, \beta)$ is independent on the upper layer thickness value $L_{R_1}$.

### *2.2.2 Parameters' identifiability*

The question of parameters' identifiability has been analysed following the principles detailed in [39]. The main hypotheses of such an analysis are:

**H1 :** The model describing the phenomeon is non-linear.

**H2 :** There is no mismatch between model and the experimental data: all important predictor variables are included in the parameter vector $\theta$ and no unimportant predictor variables are included in the parameter vector $\theta$.

**H3 :** The disturbance model is additive, normaly distributed, of zero mean (no bias), with variances $\sigma_i^2$ known for each diameter $D_i$ (so that all weighted data value are equally unreliable, see equation 13), and independent on each other.

The parameters identifiability is expressed as indifference region computed with a confidence level of 95%, meaning that:

- For a $P = 1$-parameter model, the indifference region at 95% is equivalent to predicting the value of twice the STandard Deviation (STD) of the results $\theta_{opt} =< E_{R1\,id} >$ if the same measurements were performed with a new disturbance.
- For a $P = 2$ or $P = 3$-parameter model, the indifference region at 95% is the region where another optimal solution $\theta_{opt}$ would have 95% of chance to be if the same measurements were performed with a new disturbance.

This region is defined as the $P$-dimensional domain over which the parameter vector $\theta$ verifies:

$$\Phi_{Param}(\theta, \beta) - \Phi_0 < \delta \tag{14}$$

where $\Phi_0$ is the minimum value of the cost function $\Phi_{Param}$ obtained for the optimal value $\theta_{opt}$. If the function $\frac{\Delta P_{mat\,i}}{\Delta S_{tissue}}\Big|_{sim}(\theta, \beta)$ was linear, such a domain would be an hyperelipsoïd of dimension $P$.

The threshold $\delta$ is defined using a statistical approach so that:

$$\delta = P\sigma^2 F(P, N_m - P, \alpha) \tag{15}$$

where $F(P, N_m - P, \alpha)$ is the upper $\alpha$ quantile for Fisher's $F$ distribution with $P$ and $(N_m - P)$ degrees of freedom, respectively. $\sigma^2$ is the variance of the normalized error vector in $\Phi_0$. In practice, given the definition of the function $\Phi_{Param}$ (equation 13) and hypotheses **H2** and **H3**, $\Phi_0$ should follow a chi-

squared distribution with $(N_m - P)$ degree of freedom. The unbiased variance is can thus be evaluated for each fitting as:

$$\sigma^2 = \left( \frac{\Phi_0}{N_m - P} \right) \tag{16}$$

where the unbiased variance $\sigma^2$ is computed over a normalized (reducted) error vector and has a theoretical expectation of 1. If hypotheses **H2** or **H3** were not met (model mismatch or bias in $Q_{i\ exp}$, $Q_{i\,cal}$ or $k_{ref}$, equation 12), the values of variance $\sigma^2$ will become greater than 1. The associated threshold $\delta$ (equation 15) and the indifference region would be overestimated.

During the optimization process, the theoretical constituent material apparent stiffness function $\frac{\Delta P_{mat\,i}}{\Delta S_{tissue}}\big|_{sim}$ (equation 13) is evalutated using the model reduction provided by a Principal Component Analysis (PCA) applied to a pre-calculated Finite Element (FE) database. The following section presents the FE database construction. For detailed description of model reduction using the PCA method and interpolation, the reader is kindly referred to [41].

### *2.2.3 Database definition*

To compute the minimum of the cost function $\Phi_{Param}$ (equation 13), the theoretical constituent material apparent stiffness $\frac{\Delta P_{mat\,i}}{\Delta S_{tissue}}\big|_{sim}(\theta, \beta)$ must be estimated (equation 13). At each step of the minimizing process, evaluating the cost function $\Phi_{Param}$ thus require to create $I$ different models, each with a specific combination of the four main parameters $D_i$, $L_{R_1}$, $E_{R1}$ and $E_{R0}$. To reduce the required CPU time, a database is created and interpolated. These 4 parameters can be combined to reduce the required FE database dimension from 4 to 2 as also proposed with a different philosophy in [15].

**Material stiffness contrast:** considering a material stiffness contrast ratio $\frac{E_{R1}}{E_{R0}}$, the constituent material apparent stiffness function $\frac{\Delta P_{mat\,i}}{\Delta S_{tissue}}\big|_{sim}$ can be seen as proportional to the bottom layer stiffness $E_{R0}$ (equation 17).

**Scale effect:** assuming the lower layer thickness is infinite (in practice, the total layer thickness is much greater than the aperture diameter $D_i$), the upper layer relative contribution to the shape $S_{tissue}$ is governed only by the ratio $\frac{D_i}{L_{R_1}}$ between the aperture diameter $D_i$ and upper layer thickness $L_{R_1}$; redundant $\frac{D_i}{L_{R_1}}$ ratio would provide redundant information in the FE database. This hypothesis has been confirmed numerically.

The actual FE database is thus reduced to two parameters so that:

$$\left.\frac{\Delta P_{mat\,i}}{\Delta S_{tissue}}\right|_{sim}(\theta,\beta) = E_{R0}\ f_{sim}(\frac{E_{R1}}{E_{R0}},\frac{D_i}{L_{R_1}}) \tag{17}$$

where $f_{sim}$ is an adimensional function depending on the layer stiffness contrast ratio $\frac{E_{R1}}{E_{R0}}$ and on the size ratio $\frac{D_i}{L_{R_1}}$.

### *2.2.4 FE model*

Applying these considerations, an axisymmetrical model taking in account large displacements has been defined (ANSYS APDL) with an aspiration cup diameter of $D_i = 10\ mm$ (Figure 4). To ensure the use of a unique converged mesh for all simulations in the database, $M = 20$ pre-meshed layers have been prepared at different depths $L_{layer\,m}$. The ratio $\frac{D_i}{L_{R_1}}$ is modified between simulations by attributing a Young's Modulus of $E_{R1}$ to the first $[1,\, m]$ pre-meshed upper-layers and a Young's modulus of $E_{R0\,ref}$ to the other layers in $[m+1,\, M]$.

The following additional parameters in vector $\beta$ have been chosen for the FE simulation:

- An **Incompressible Neo-Hookean model** simulates the material behavior of each layer. The constituent material apparent stiffness $\frac{\Delta P_{mat\,i}}{\Delta S_{tissue}}\big|_{sim}$ is evaluated at shapes equal to 0.1; for such a small deformation state, the material incompressibility (Poisson coefficient $\nu \in [0.45\ 0.5[$) has no influence onto the results (numerically tested).
- **Aspiration cup geometry** in contact with the sample is representative of the reality (wall thickness, fillet radius). $3D$ printed cup parts in contact with the tissue are proportional to the cup aperture $D_i$.
- **Boundary conditions:** the cup itself is immobilized in all directions on line $CD$ (Figure 4). Contact elements are created between the line $AB$ on the tissue and the cup (zoom-in in Figure 4). Partial vacuum (pressure noted $-P_{mat}$) is applied on line $AB$ including the line part beneath the cup contact. With these boundary conditions, the tissue sample is free to move up or down relatively to the cup according to the applied pressure $-P_{mat}$. The line $AB$ displacement versus pressure $-P_{mat}$ is post-processed to compute the aspirated shape $S_{tissue}$ (equation 9). The slope $\frac{\Delta P_{mat\,i}}{\Delta S_{tissue}}\Big|_{sim}$ is computed at shape $S_{tissue} = 0.1$, which provides in turn the adimensional value $f_{sim}$ (equation 17).
- The **friction coefficient** between tissue and cup is chosen of $f = 0.2$. During the experiment, this parameter is actually an unknown and is affected by the ultrasound gel cord. The friction coefficient influence has been tested numerically (no friction to glued boundary conditions). Its effect was considered negligible (as also reported in [42]) when the upper layer is stiffer than the lower layer.
- **External loads applied on the cup** are as small as possible during the experiments (Figure 6, illustration on sample $A$). No additional external loads are considered in the simulation. This hypothesis will be discussed while analyzing the results.

- The **tissue sample size** in the model is chosen so that rigid or free boundary conditions applied on the tissue outer boundaries have negligible influence onto the sought function (numerically tested).
- **Mesh convergence** : The layers are meshed using 8 nodes elements ($Q8$, Plane183, ANSYS). The mesh convergence has been checked on the tissue shape prior to the database simulation, the mesh being the same for all simulations. A zoom-in of the meshing size is reported in Figure 4.

#### *2.2.5 Database range and interpolation*

The FE database has been computed on stiffnesses ratios ranges: $\frac{E_{R1}}{E_{R0}} \in [0.1\ 120]$ and $\frac{D_i}{L_{R_1}} \in [0.33\ 133]$ (Figures 4 and 5).

A PCA is applied to the database to extract eigenvectors and weighting functions. Only the 3 first eigen-vectors and associated weighting functions were kept, representing more than 99.99% of the database information. Eigen vectors and weighting functions were both interpolated with splines to compute $f_{sim}$ (equation 17, Figure 5).

### 2.3 Controlled bi-layer silicone specimens

To validate the method, bi-layered specimens made of two mechanically characterized $R_0$ (soft) and $R_1$ (stiffer) silicones were tested.

These silicones were obtained mixing equal mass of component $A$ and $B$[d] and adding silicone softener[e] (14.6% of $(A+B)$ mass for $R_1$, 30% of $(A+B)$ mass for $R_0$). The mixed silicones were vacuumed during 5 $min$ to remove air bubbles before pouring.

Three types of samples were made:

[d] Skin FX10 110019
[e] Deadner Skin FX10 110020

- **Homogenous aspiration specimens:** simple cylinders of $\varnothing 96\ mm \times 70\ mm$ used as references and labelled $R_0$ and $R_1$ (Figure 6a).
- **Bi-layered aspiration specimens:** cylinders of $\varnothing 96\ mm$, with thick $R_0$ bottom layer (soft), and thin upper $R_1$ layer (stiffer) of thickness $L_{R_1}$ ($A$ to $E$, Figure 6a). The samples were molded upside-down: the $R_1$ stiffer layer was molded first controling the poured volume with a syringe, followed one hour later by the softer layer of $R_0$.

  The upper layer thicknesses $L_{R_1\,pic}$ were measured after all aspiration tests by cutting the samples in half and taking magnified scale controlled pictures. Thicknesses were evaluated in 8 different locations
- **Flat tensile specimens:** 5 to 10 flat specimens ($40 \times 160 \times 3\ mm^3$ molds) were molded from the same mixes as the aspiration samples. The averaged section $A_0$ of these samples are estimated by weighting each specimen mass $m_{tens}$ so that $m_{tens} = \rho\, b\, A_0$ with $\rho$ the silicone volumetric mass and $b$ the mold length.

The tensile specimens Young's Moduli $E_{R1\,tens}$ and $E_{R0\,tens}$ were evaluated during quasi-static uniaxial tensile tests on a MTS tensile machine.

## 3 Results

### 3.1 Reference values

The tensile results on the $R_0$ and $R_1$ flat specimens are presented in Figure 6b. Fitting a Neo-Hookean incompressible model onto the tensile curves for $\lambda_1 = \frac{L}{L_0} \in [1, 1.1]$ provides Young's moduli of $E_{R1\,tensile} = 74.7 \pm 2.3\ kPa$ and $E_{R0\,tensile} = 8.97 \pm 0.64\ kPa$ where the tolerance interval is given as twice the experimental STD (Table 1). The stiffness ratio $\frac{E_{R1\,tensile}}{E_{R0\,tensile}}$ is equal to 8.3.

The optically measured thicknesses $L_{R_1\,pic}$ of reference samples are presented in Table 2. Errors intervals are given as twice the experimental STD.

| Flat tensile specimens | $\mathbf{E_{tensile}}$ (kPa) |
|---|---|
| $R_0$ | **9.0** [8.3 , 9.6] |
| $R_1$ | **74.7** [72.4 , 77.0] |

**Table 1** Reference values: identified Young Moduli from tensile test on flat specimens.

| Aspiration specimens | $R_1$ layer thickness $L_{R_1\,pic}$ |
|---|---|
| $R_0$ | 0 mm |
| $A$ | 1.08±0.064 mm |
| $B$ | 3.27±0.06 mm |
| $C$ | 6.22±0.055 mm |
| $D$ | 9.16±0.076 mm |
| $E$ | 11.75±0.05 mm |
| $R_1$ | 69 mm |

**Table 2** Reference values: layer thicknesses $L_{R_1\,pic}$ evaluated by an annex destructive measurement.

### 3.2 Aspiration settings

The cup was held into place while minimizing external loads applied to the cup thanks to a special 3D printed holder[f] (Figure 6a, applied to specimen $A$).

The volumes of air withdrawn from the reference and material lines $\Delta V$ was of 0.1 $mL$ and kept identical for all the cups diameters $D_i$. A complete cycle (withdrawing and injecting $\Delta V$) was of about 10 seconds. A total of 5 cycles were performed during each acquisition (intra-test reproducibility). Each test has been performed 2 to 3 times (inter-test reproducibility).

[f] 3D printer Prusa MK3S+

The pressure-pressure curve $\Delta P_{mat}$-$\Delta P_{ref}$ was monitored during all the tests; tests with leakage were identified when pressure $P_{mat}$ drifted cycle after cycle. Such tests were immediately discarded.

Only pressure signals obtained during $\Delta V$ withdrawing and for $\Delta V_{syringe} > 0.01\ mL$ were used to evaluate $Q_{i\,exp}$ (equation 6) to avoid impact of possible syringe piston asymmetrical behavior during movement inversion in the reference and material lines.

### 3.3 Constituent material apparent stiffnesses: $\left.\frac{\Delta P_{mat\,i}}{\Delta S_{tissue}}\right|_{exp}$

The experimental constituent material apparent stiffnesses $\left.\frac{\Delta P_{mat\,i}}{\Delta S_{tissue}}\right|_{exp}$ (equation 12) for each cycle are presented versus the aperture diameter $D_i$ in Figure 7 a. Taking advantage that the thicknesses $L_{R1\,pic}$ are measured during an annex measurement (Table 2), the experimental constituent material apparent stiffness $\left.\frac{\Delta P_{mat\,i}}{\Delta S_{tissue}}\right|_{exp}$ are also plotted versus the ratio $\frac{D_i}{L_{R1\,pic}}$ in Figure 7 b.

### 3.4 Optimal identified parameter $\theta$ and indifference regions

For illustration purpose, details of fitted curves and indifference regions are presented on sample B (Figure 8).

Aspiration results on specimens $R_0$ and $R_1$ for $P = 1$ are summarized in table 3 with direct comparisons to the tensile reference values.

| | | Aspiration test |
|---|---|---|
| $\mathbf{P = 1}$ | $\sigma^2$ | $\mathbf{E_{opt}}$ (kPa) |
| $R_0$ | 367 | **11.7** (*+29.9%*) [11.5 , 11.9] |
| $R_1$ | 7.9 | **78.9** (*+5.6%*) [78.7 , 79.1] |

**Table 3** Identified Young Moduli from aspiration data on homogeneous specimens for the $P = 1$-parameter model are in **bold**. The Relative Error (RE) between optimal aspiration and reference value is in (*italic*). Values in bracket are the minimum and maximum values of the indifference region at 95% for each parameter identified with aspiration.

Aspiration results on specimens $A$ to $B$ are summarized in table 4 for $P = 2$ and 3 with direct comparisons to the reference values.

| **P = 2** | $\sigma^2$ | $\mathbf{L_{R_1\ pic}}$ (mm) | $\mathbf{E_{R_1\ opt}}$ (kPa) | $\mathbf{E_{R_0\ opt}}$ (kPa) |
|---|---|---|---|---|
| *A* | 71 | **1.08**±0.064 | **96.4** (*+29.1%*) [81.3 , 113.2.0] | **8.8** (*-2.5%*) [8.4 , 9.1] |
| *B* | 32 | **3.27**±0.060 | **80.7** (*+8.0%*) [78.3 , 83.3] | **8.9** (*-1.0%*) [8.5 , 9.3] |
| *C* | 7 | **6.22**±0.042 | **80.0** (*+7.1%*) [79.6 , 80.9] | **12.0** (*33.8%*) [11.7 , 12.8] |
| *D* | 15 | **9.16**±0.076 | **79.7** (*+6.7%*) [79.3 , 80.3] | **12.5** (*39.3%*) [11.6 , 13.7] |
| *E* | 10 | **11.75**±0.050 | **79.3** (*+6.1%*) [79.0 , 79.6] | **11.6** (*28.6%*) [10.3 , 13.2] |
| **P = 3** | $\sigma^2$ | $\mathbf{L_{R_1\ opt}}$ (mm) | $\mathbf{E_{R_1\ opt}}$ (kPa) | $\mathbf{E_{R_0\ opt}}$ (kPa) |
| *A* | 62 | **1.51** (*+39.5%*) [1.51 , 1.76] | **57.5** (*-23.1%*) [46.82 , 76.2] | **8.4** (*-6.8%*) [7.9 , 8.9] |
| *B* | 31 | **3.26** (*-0.33%*) [3.09 , 3.44] | **80.9** (*+8.4%*) [77.0 , 85.5] | **8.9** (*-0.6%*) [8.3 , 9.5] |
| *C* | 3 | **5.52** (*-11.2%*) [5.39 , 5.67] | **83.2** (*+11.4%*) [82.4 , 84.0] | **15.3** (*+70.2%*) [14.5 , 16.04] |
| *D* | 13 | **8.37** (*-8.5%*) [7.55 , 9.08] | **80.7** (*+8.1%*) [79.7 , 82.1] | **16.5** (*+83.8%*) [12.8 , 20.9] |
| *E* | 6 | **8.85** (*-24.7%*) [7.91 , 9.66] | **80.9** (*+8.3%*) [80.2 , 81.8] | **27.8** (*+209.3%*) [23.4 , 32.7] |

**Table 4** Identification results for the $P = 2$ and $P = 3$-parameter models: the optimal value using aspiration data is in **bold**. The Relative Error (RE) between optimal aspiration and reference value is in (*italic*). Values in bracket are the minimum and maximum values of the indifference region at 95% for each parameter identified with aspiration. Color code: green if $|RE| < 15\%$, orange if $15\% < |RE| < 30\%$, red if $|RE| > 30\%$.

A more global summary is graphically represented in Figure 9 to highlight the indifference regions variations depending on the tested sample ($A$ to $E$) and value of parameter $P$. Results obtained on homogeneous samples ($P = 1$) and by tensile tests are reported as horizontal red, blue and black bands of twice the experimental STD (indifference regions at 95%).

## 4 Discussion

Given that only two silicone mixes $R_1$ and $R_0$ were used, the stiffness ratio $\frac{E_{R1}}{E_{R0}} \approx 8.3$ is identical for aspiration specimens $A$ to $E$.

- This corresponds to a unique curve of the FE database (equation 17). The database stiffnesses ratios range of $\frac{E_{R1}}{E_{R0}} \in [0.1\ 120]$ is thus overkill but was chosen to allow computation of large indifference regions and to anticipate

application to human skin, with hypodermis tissues that are much softer than the dermis/epidermis layer.

- The experimental curves overlap in Figure 7b confirms this stiffness ratio uniqueness is also observed experimentally with the aspiration tests; this is a qualitative assessment of the experimental measurement quality of both $\left.\frac{\Delta P_{mat\,i}}{\Delta S_{tissue}}\right|_{exp}$ and $L_{R1\,pic}$. Depending on the layer thickness $L_{R1}$, the aperture diameters from 4 to 30 $mm$ extract different parts of the curve.

4.1 Homogeneous aspiration samples, $P = 1$-parameter model:

**Stiffer $R_1$ silicone:** the measurement $\left.\frac{\Delta P_{mat\,i}}{\Delta S_{tissue}}\right|_{exp}$ is almost independent on the aperture diameter $D_i$ (Figure 7a, red curve) which is in accordance with theory for a upper layer thickness greater or equal to the maximal aperture diameter [15]. The aspiration test over-estimates the $R_1$ Young Modulus compared to the tensile result $E_{R1\,tensile}$ by 5.6% (Table 3), which is the same order of magnitude as in [30].

**Softer $R_0$ silicone:** The aspiration test with the $P = 1$-parameter model over-estimates the $R_0$ Young Modulus compared to the tensile one $E_{R0\,tensile}$ by 29.9%. The fitting score of $\sigma^2 = 367$ is far from the expected value of 1 (Table 3). This poor fitting score is due to the fact that the measurement $\left.\frac{\Delta P_{mat\,i}}{\Delta S_{tissue}}\right|_{exp}$ increases for small $D_i$ (Figure 7a, blue lowest curve). This behavior was not expected for an homogeneous sample. A possible explanation is that soft materials are very sensitive to normal loading applied to small cups [43]. Such an initial load makes the material surface to be curvaceous, which replaces some air into the cup by material before closing the system valve. The used calibration value $Q_{i\,cal}$, measured on a flat undeformable surface, is thus larger than reality. This bias induces an over-

estimation of the measurement $\frac{\Delta P_{mati}}{\Delta S_{tissue}}\big|_{exp}$ (equation 8). This phenomena should yet be limited by the presence of the holding system (Figure 6a).

4.2 Bi-layer aspiration sample, $P = 2$ or 3-parameter models:

The computed indifference region sizes are in accordance with "ill-posedness" aspect of the tested case:

- Sample $A$ has a very thin upper layer of 1.08 $mm$. Aperture diameters from 4 to 30 $mm$ are thus well adapted to extract information about the lower layer stiffness $E_{R_0}$. Relative Errors with tensile test ($-2.5$ and $-6.8\%$ for $P = 2$ or $P = 3$-parameter models, respectively, table 4) and indifference regions lower than 1 $kPa$ on $E_{R_0}$ confirm this observation.

  The smallest aperture diameter being 4 times larger than the upper layer thickness, the upper modulus $E_{R1}$ is the least well identified among the tested samples (relative error of $+29.1$ and $-23.1\%$ for $P = 2$ or $P = 3$-parameter models, respectively, table 4), which is pointed out by aspiration indifference region greater than 32 $kPa$ on $E_{R_1}$.
- Sample $B$, with an upper layer of 3.27 mm is the most adapted among the made samples to provide both proper upper and lower layer moduli given the used aperture diameters range ($|RE| < 15\%$ for all optimal values and for both $P = 2$ and 3-parameter models, table 4). The computed indifference regions are of about 5 $kPa$ for the upper modulus $E_{R1}$ and 1 $kPa$ for the lower modulus $E_{R0}$. This highlights the identification robustness even though the residual error vector shows that hypotheses **H2** and **H3** are not experimentally met and $\sigma^2 = 31$ is far from the expected value of 1 (Figure 8c). The knowledge of the upper layer thickness is thus not mandatory when the layer thickness is well adapted to the used aperture diameter range.

- Samples $C$ to $E$, with layers thicker than 6 mm, provide proper upper layer modulus $E_{R1}$ identification and indifference regions of the order of 1 $kPa$ for $P = 2$ or $P =$ 3-parameter models (RE lower than 15%); the upper layer thickness knowledge is not mandatory in this case.

  As expected, the lower layer modulus $E_{R0}$ identifiability decreases as the upper layer thickness increases ($RE > 30\%$ and increasing with the layer thickness $L_{R_1\,pic}$), which is pointed out by indifference region increasing from 1 to 10 $kPa$. Knowing the upper layer thickness improves the identification but the RE remains around 30%.

From a practical point of view, the upper layer thickness knowledge is thus not mandatory: when this value is known ($P =$ 2-parameter model), the obtained RE is stabilized but not fully satisfactory for the lower layer modulus $E_{R0}$ identification; identifications results are considered similar with both $P = 2$ and 3-parameter models.

## 5 Limitation/Perspectives

The current system hardware, experimental and identification method provide satifactory results. Some limitations and associated perspectives should be yet be mentioned in anticipation of application to skin measurements:

### 5.1 Hardware limitation

The same volume $\Delta V$ is cyclically withdrawn from the "Material line" for all aperture diameter $D_i$. The maximal shape reached for small cups is thus larger than for large diameters. This has no impact while analysing linear materials but should be taken into account while applying the method to non-linear materials (stiffening for example). Being able to adjust the withdwan volume $\Delta V$ with the diameter size would be advisable.

### 5.2 Protocole limitation

The aperture diameter is applied onto a flat surface and held in place with the lowest possible intial load. In any other case, the tissue sample will be initially curveous into the aspiration chamber. This would modify the reference air quantity into the systeme and associated calibration curve; a bias would be added to the experimental result. Morevoer, the surface curvature shall impact airthigness for large aperture diameter cups, preventing their use. Eventually, performing measurements *in vivo* will provide noisier data (breathing, muscle activation,*etc*) averaged over the cycles. These phenomena impact onto the whole identification process should be evaluated.

### 5.3 Inverse analyse limitation

Identification is performed using a linear model for both the system lines (including the tested tissue, equations 1 to 3), reducing the extracted mechanical parameters to the layers' Young Moduli. More complexe behavior should be considered to extract richer model parameters such as stiffening of the upper layer for example. Second, the two layer thickness is considered much bigger than the aperture diameter $D_i$. Such a parameter should be satisfied experimentally. If not, a FE database adapted to this situation should be evaluated.

## 6 Conclusion

A clinically friendly aspiration system has been developed. Cyclic partial vacuum is applied to the tested tissue to evaluate its apparent mechanical properties at very low deformation. The system aspiration cup can easily be switched for aperture diameters $D_i$ between 4 and 30 mm. The developed identification method enables, almost in real-time, to

- identify mechanical Young moduli and the upper layer thickness of bi-layered structures using an off-line Finite Element database,
- evaluate indifference regions (prediction of standard deviation) for each identified parameter given the experimental results,

The system was tested *in silico* on controlled bilayer specimens for upper layer thicknesses from 1 to 12 mm. The bilayer sample with an upper layer of 3 mm presented the best parameter identifiability for both Young's moduli (relative errors lower than 10% compared to reference values obtained during tensile tests). The upper layer thickness was also identified with an error lower than 2%. On other upper layer thicknesses, identified results were of the proper order of magnitude. The obtained indifferences regions in each cases were representative of the identification quality and "ill-posedness" of the experimental situation.

These results provide hope to apply the method to human skin for which the $L_{layer}$ range is compatible (Bmode US scanner used to identify visually the dermis and hypodermis interface, 1.36 to 3.5 $mm$ on head skin [16]).

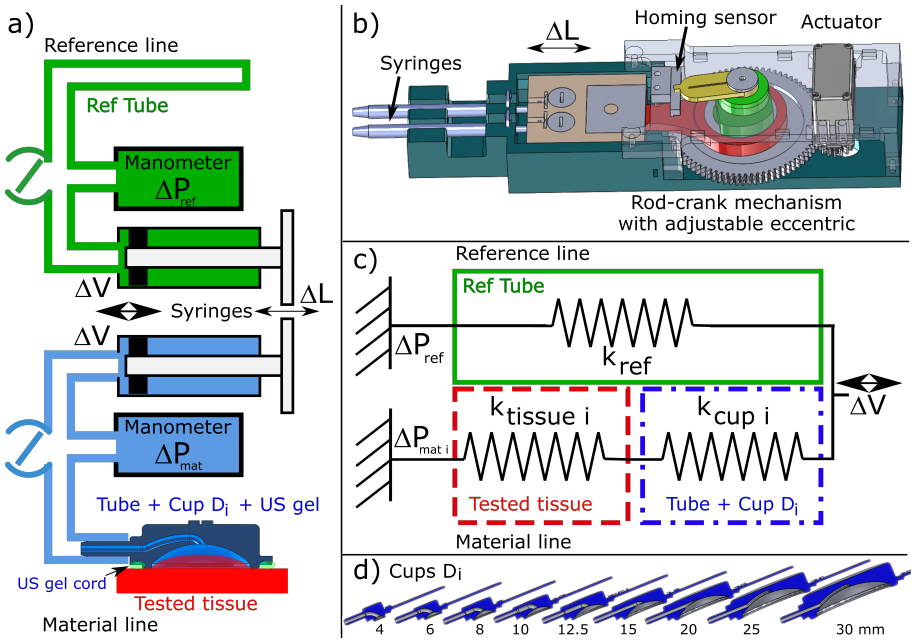


**Fig. 2 Subplot a)** Principle of the two lines system to evaluate the material mechanical answer of soft tissues during cyclic aspiration.
**Subplot b)** Syringes cyclic actuator with adjustable screw-driven eccentric and homing sensor.
**Subplot c)** Equivalent spring model of the whole system.
**Subplot d)** Aspiration cups with aperture diameters ranging from 4 to 30 *mm*.

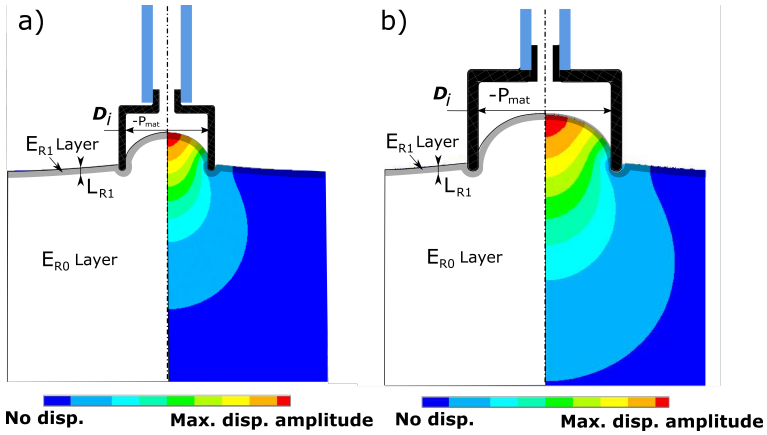


**Fig. 3** Illustration of aspiration on a bi-layer sample using different aperture diameters for $S_{tissue} = 1$. The colors under the cups schematically represent the material volume over which the material stiffness information is extracted. Changing the aspiration diameter $D_i$ modifies the relative contribution of the upper layer to the final shape $S_{tissue}$.

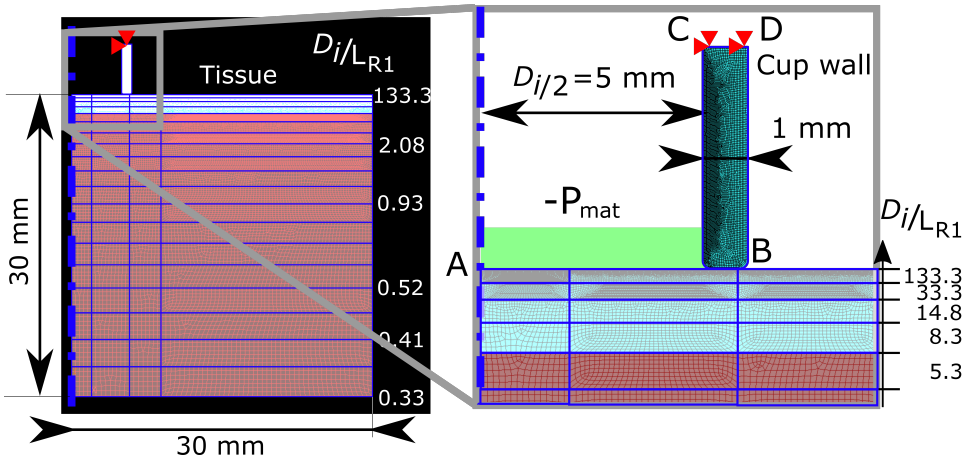


**Fig. 4** Axisymmetrical FE model geometry. Zero displacements are presented as red triangles. Partial vacuum homogeneous pressure is represented by the green rectangle in the zoom in subplot. Pre-meshed layers are defined at different depths to use the same converged mesh for all calculations. Material mechanical properties $E_1$ is applied to elements of the upper pre-meshed layers (illustration for a ratio $\frac{D_i}{L_{R_1}} = 8.3, m = 4$).

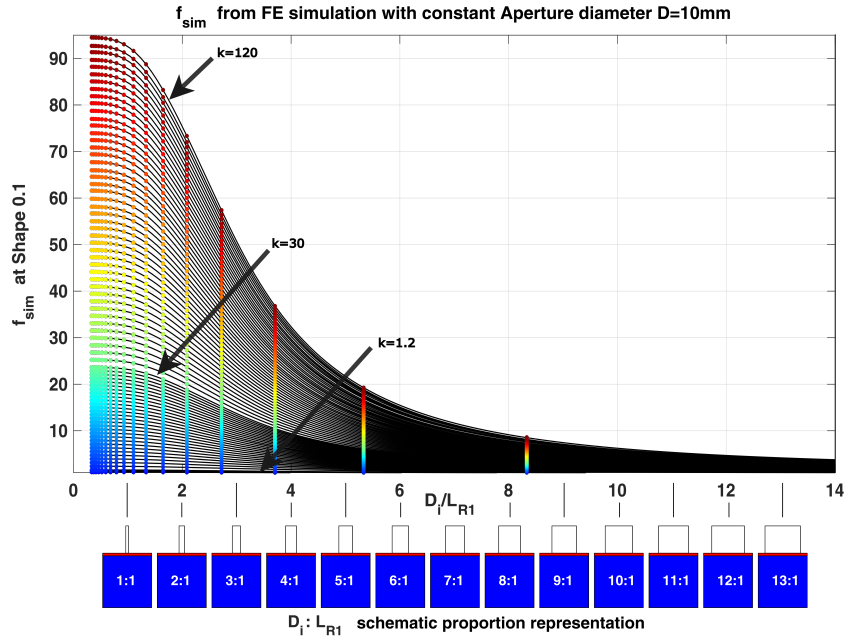


**Fig. 5** The FE normalized results stored in the database are represented as points (computed at shape $S_{tissue} = 0.1$) versus depths ratio $\frac{D_i}{L_{R_1}}$. The stiffnesses ratios range is $k = \frac{E_{R1}}{E_{R0}} \in [1.2\ 120]$. The PCA interpolation enables to interpolate the database, as presented with the black curves. The meaning of the depths ratio $\frac{D_i}{L_{R_1}}$ is visually represented for integer values under the abscisse axis.

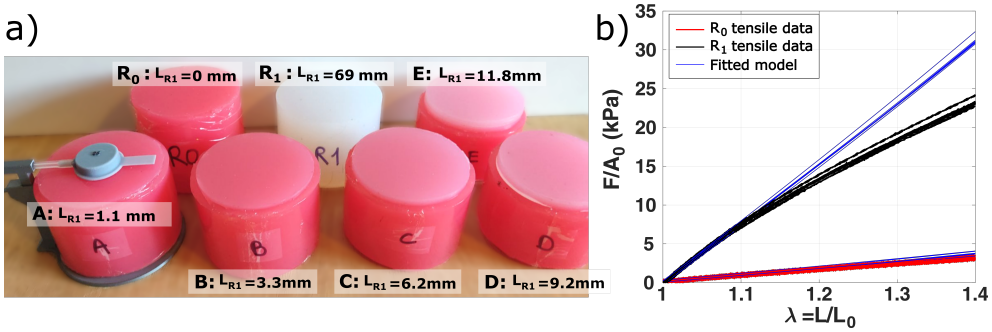


**Fig. 6 Subplot a)** Homogeneous ($R_0$ and $R_1$) and bi-layered aspiration samples ($A$ to $E$) made with stiffer $R_1$ silicone as upper layer (white) and softer $R_0$ silicone as bottom layer (pink).
**Subplot b)** Tensile test results on flat rectangular specimens ($40 \times 160 \times 3\ mm^3$). Softer $R_0$ silicone (red curve) and stiffer $R_1$ silicone (black curve). Associated Neo Hookean curve fitting using data over the domain for $\lambda_1 = \frac{L}{L_0} \in [1, 1.1]$.

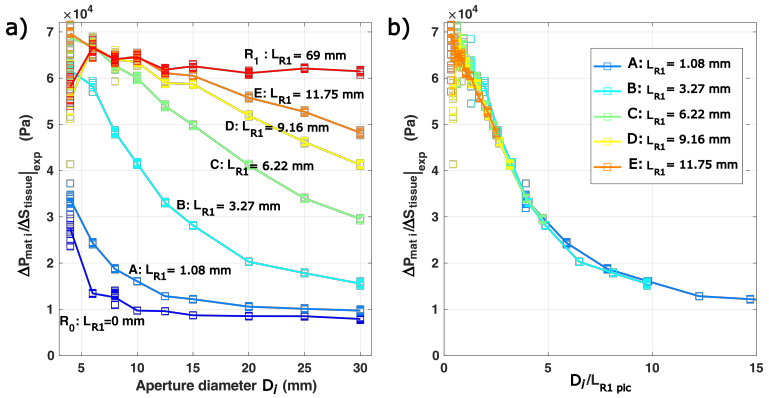


**Fig. 7** Experimental results $\frac{\Delta P_{mat\,i}}{\Delta S_{tissue}}\big|_{exp}$ on bi-layered and homogenous specimens (Table 2): **subplot a)** Plot versus aperture diameter $D_i$, **subplot b)** Plot versus ratio $\frac{D_i}{L_{R1\,pic}}$ where $L_{R1\,pic}$ is evaluated during an annex destructive measurement.

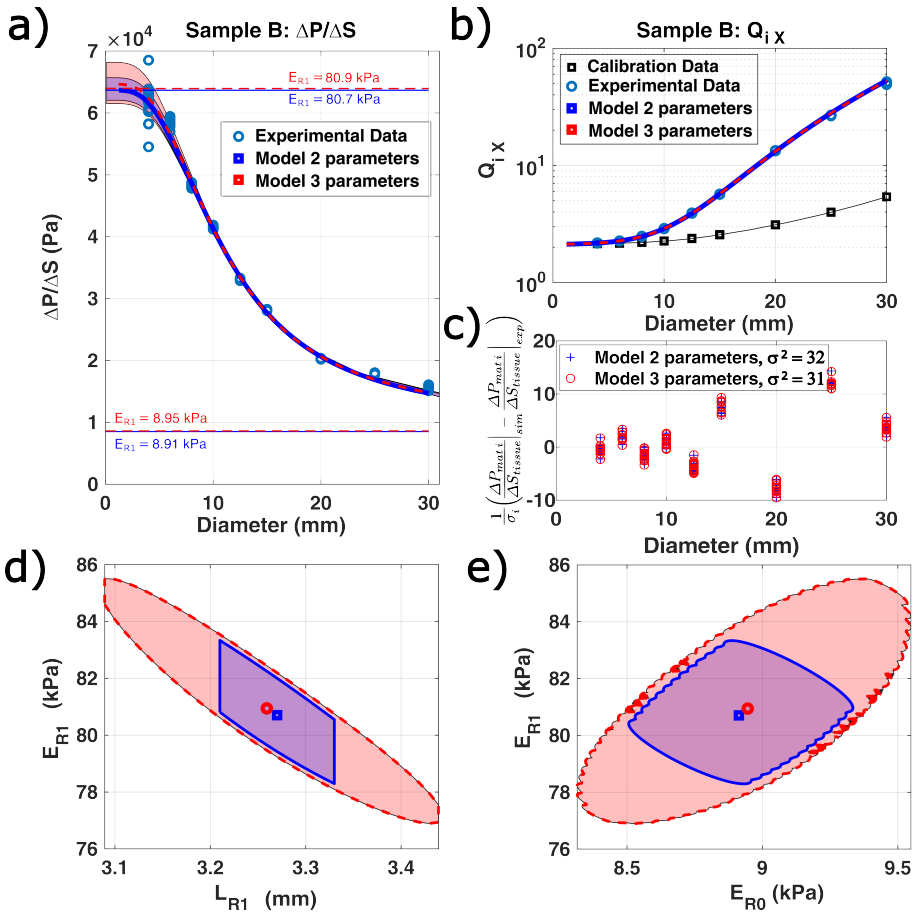


**Fig. 8** Experimental data and inverse identification on sample $B$.
**Subplot a)** Experimental material apparent stiffnesses $\frac{\Delta P_{mat\,i}}{\Delta S_{tissue}}\Big|_{exp}$, best fitted curves and swept area for parameters in the $P$-dimensional indifference region. For homogeneous samples, values of $\frac{\Delta P_{mat\,i}}{\Delta S_{tissue}}\Big|_{sim}$ are independent on the aperture diameter. Such cases are represented as dashed horizontal lines corresponding to the optimal identified upper and lower material Young Moduli ($E_{R1\,opt}$ and $E_{R0\,opt}$).
**Subplot b)** Calibration $Q_{i\,cal}$ and experimental $Q_{i\,exp}$ values (equation 5) versus aperture diameter $D_i$. The calibration curve represents the aspiration results obtained onto an infinitely stiff material. Note that the ordinate is in log scale.
**Subplot c)** Optimized reducted error vectors $\frac{1}{\sigma_i}\left(\frac{\Delta P_{mat\,i}}{\Delta S_{tissue}}\Big|_{exp} - \frac{\Delta P_{mat\,i}}{\Delta S_{tissue}}\Big|_{sim}\right)$ to compute $\Phi_0$ (equation 13) for both $P = 2$ and $P = 3$-parameter models. Note that the error spread is similar for each diameter $D_i$ thanks to the use of the weighting factor $\frac{1}{\sigma_i}$. The hypothesis of a disturbance with no bias is not experimentally met here, explaining the "unsatisfactory" value $\sigma^2 = 32$ for both $P = 2$ and $P = 3$-parameter models.
**Subplots d)** The markers and areas represent optimal identified Young moduli $E_{R1}$ versus layer thickness $L_{R_1}$ and associated indifference regions in the cases $P = 2$ (assuming a layer thickness $L_{R_1\,pic} = 3.27 \pm 0.05\ mm$, Table 2) and $P = 3$, respectively.
**Subplots e)** The markers and areas represent optimal identified Young moduli $E_{R1}$ and $E_{R0}$ and associated indifference regions in the cases $P = 2$ (assuming a layer thickness $L_{R_1\,pic} = 3.27 \pm 0.05\ mm$, Table 2) and $P = 3$, respectively. Such good areas overlaping is not met for all specimens and depends on the closeness between the optimal layer thickness $L_{R_1}$ and actual layer thickness $L_{R_1\,pic}$.

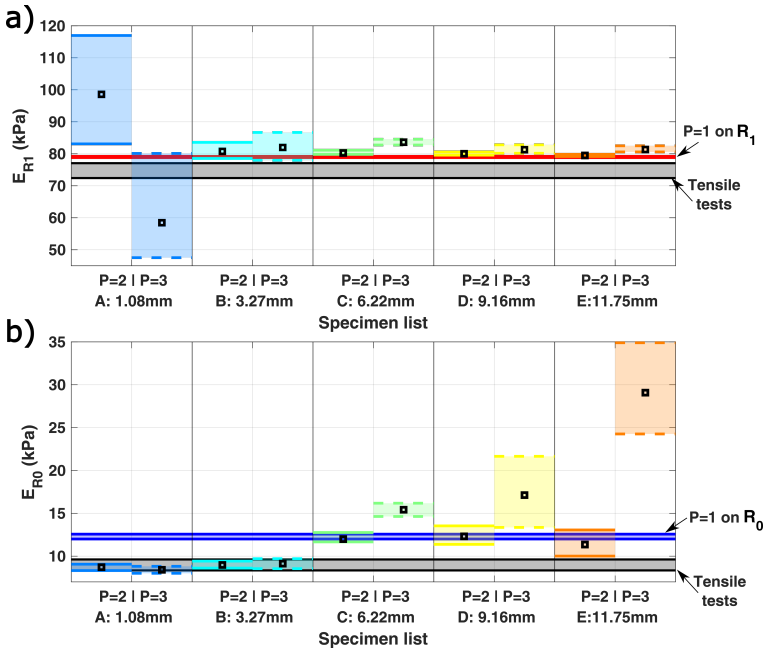


**Fig. 9** Experimental indifference ranges on samples $A$ to $E$:
**Subplot a)** Identification ranges for the upper layer $R_1$ using a $P = 2$ or $P = 3$-parameters model. The horizontal black band represents the tensile test indifference region at 95% (average $\pm$ 2 Std) on silicones $R_1$. The horizontal red band represents the 95% indifference region on aspiration using a $P = 1$-parameter model on the homogeneous sample $R_1$.
**Subplot b)** Identification ranges for the lower layer $R_0$ using a $P = 2$ or $P = 3$-parameters model. The horizontal black band represents the tensile test indifference region at 95% (average $\pm$ 2 Std) on silicones $R_0$. The horizontal blue band represents the 95% indifference region on aspiration using a $P = 1$-parameter model on homogeneous samples $R_0$.

## References


1. Y. Fung, *Biomechanics: Mechanical Properties of Living Tissues*. Springer New York, 1981.
2. Y. Payan, ed., *Soft Tissue Biomechanical Modeling for Computer Assisted Surgery*. Springer Berlin, 2012.
3. A. E. Kerdok, M. P. Ottensmeyer, and R. D. Howe, "Effects of perfusion on the viscoelastic characteristics of liver," *Journal of Biomechanics*, vol. 39, no. 12, pp. 2221–2231, 2006.
4. M. P. Ottensmeyer, "In vivo measurement of solid organ visco-elastic properties," *Studies in health technology and informatics*, pp. 328–333, 2002.
5. A. Gefen and S. S. Margulies, "Are in vivo and in situ brain tissues mechanically similar?," *Journal of biomechanics*, vol. 37, no. 9, pp. 1339–1352, 2004.
6. E. Girard, G. Chagnon, E. Gremen, M. Calvez, C. Masri, J. Boutonnat, B. Trilling, and B. Nottelet, "Biomechanical behaviour of human bile duct wall and impact of cadaveric preservation processes.," *Journal of the mechanical behavior of biomedical materials*, vol. 98, pp. 291–300, 2019.
7. S. Budday, G. Sommer, C. Birkl, C. Langkammer, J. Haybaeck, J. Kohnert, M. Bauer, F. Paulsen, P. Steinmann, E. Kuhl, *et al.*, "Mechanical characterization of human brain tissue," *Acta biomaterialia*, vol. 48, pp. 319–340, 2017.
8. C. Masri, G. Chagnon, D. Favier, H. Sartelet, and E. Girard, "Experimental characterization and constitutive modeling of the biomechanical behavior of male human urethral tissues validated by histological observations," *Biomechanics and modeling in mechanobiology*, vol. 17, no. 4, pp. 939–950, 2018.

9. Z. Gao, K. Lister, and J. P. Desai, "Constitutive modeling of liver tissue: experiment and theory," *Annals of biomedical engineering*, vol. 38, no. 2, pp. 505–516, 2010.
10. R. Avazmohammadi, D. S. Li, T. Leahy, E. Shih, J. S. Soares, J. H. Gorman, R. C. Gorman, and M. S. Sacks, "An integrated inverse model-experimental approach to determine soft tissue three-dimensional constitutive parameters: application to post-infarcted myocardium," *Biomechanics and modeling in mechanobiology*, vol. 17, no. 1, pp. 31–53, 2018.
11. T. K. Tonge, L. S. Atlan, L. M. Voo, and T. D. Nguyen, "Full-field bulge test for planar anisotropic tissues: Part i–experimental methods applied to human skin tissue," *Acta biomaterialia*, vol. 9, no. 4, pp. 5913–5925, 2013.
12. M. Diab, N. Kumaraswamy, G. P. Reece, S. E. Hanson, M. C. Fingeret, M. K. Markey, and K. Ravi-Chandar, "Characterization of human female breast and abdominal skin elasticity using a bulge test.," *Journal of the mechanical behavior of biomedical materials*, vol. 103, p. 103604, 2020.
13. A. Samani, J. Zubovits, and D. Plewes, "Elastic moduli of normal and pathological human breast tissues: an inversion-technique-based investigation of 169 samples," *Physics in medicine & biology*, vol. 52, no. 6, p. 1565, 2007.
14. M. A. Cox, N. J. Driessen, R. A. Boerboom, C. V. Bouten, and F. P. Baaijens, "Mechanical characterization of anisotropic planar biological soft tissues using finite indentation: experimental feasibility," *Journal of biomechanics*, vol. 41, no. 2, pp. 422–429, 2008.
15. R. Zhao, K. L. Sider, and C. A. Simmons, "Measurement of layer-specific mechanical properties in multilayered biomaterials by micropipette aspiration," *Acta biomaterialia*, vol. 7, no. 3, pp. 1220–1227, 2011.

16. M. Xu and J. Yang, "Human facial soft tissue thickness and mechanical properties: a literature review," in *International Design Engineering Technical Conferences and Computers and Information in Engineering Conference*, vol. 57045, p. V01AT02A045, American Society of Mechanical Engineers, 2015.
17. S. Diridollou, F. Patat, F. Gens, L. Vaillant, D. Black, J. Lagarde, Y. Gall, and M. Berson, "In vivo model of the mechanical properties of the human skin under suction," *Skin Research and technology*, vol. 6, no. 4, pp. 214–221, 2000.
18. F. Hendriks, D. Brokken, C. Oomens, D. Bader, and F. Baaijens, "The relative contributions of different skin layers to the mechanical behavior of human skin in vivo using suction experiments," *Medical engineering & physics*, vol. 28, no. 3, pp. 259–266, 2006.
19. S. Badir, M. Bajka, and E. Mazza, "A novel procedure for the mechanical characterization of the uterine cervix during pregnancy," *Journal of the mechanical behavior of biomedical materials*, vol. 27, pp. 143–153, 2013.
20. A. Nava, E. Mazza, M. Furrer, P. Villiger, and W. Reinhart, "In vivo mechanical characterization of human liver," *Medical image analysis*, vol. 12, no. 2, pp. 203–216, 2008.
21. V. Luboz, E. Promayon, and Y. Payan, "Linear elastic properties of the facial soft tissues using an aspiration device: towards patient specific characterization," *Annals of biomedical engineering*, vol. 42, no. 11, pp. 2369–2378, 2014.
22. M. Kauer, V. Vuskovic, J. Dual, G. Székely, and M. Bajka, "Inverse finite element characterization of soft tissues," *Medical Image Analysis*, vol. 6, no. 3, pp. 275–287, 2002.
23. P. Schiavone, F. Chassat, T. Boudou, E. Promayon, F. Valdivia, and Y. Payan, "In vivo measurement of human brain elasticity using a light

aspiration device," *Medical image analysis*, vol. 13, no. 4, pp. 673–678, 2009.

24. M. Hollenstein, G. Bugnard, R. Joos, S. Kropf, P. Villiger, and E. Mazza, "Towards laparoscopic tissue aspiration," *Medical image analysis*, vol. 17, no. 8, pp. 1037–1045, 2013.
25. J. Weickenmeier, M. Jabareen, and E. Mazza, "Suction based mechanical characterization of superficial facial soft tissues," *Journal of biomechanics*, vol. 48, no. 16, pp. 4279–4286, 2015.
26. B. Röhrnbauer, C. Betschart, D. Perucchini, M. Bajka, D. Fink, C. Maake, E. Mazza, and D. A. Scheiner, "Measuring tissue displacement of the anterior vaginal wall using the novel aspiration technique in vivo," *Scientific reports*, vol. 7, no. 1, pp. 1–7, 2017.
27. V. Vuskovic, *Device for in-vivo measurement of mechanical properties of internal human soft tissues*. PhD thesis, ETH Zurich, 2001.
28. P. Lakhani, K. K. Dwivedi, A. Parashar, and N. Kumar, "Non-invasive in vivo quantification of directional dependent variation in mechanical properties for human skin," *Frontiers in Bioengineering and Biotechnology*, vol. 9, 2021.
29. S. A. Elahi, N. Connesson, and Y. Payan, "Disposable system for in-vivo mechanical characterization of soft tissues based on volume measurement," *Journal of Mechanics in Medicine and Biology*, vol. 18, no. 04, p. 1850037, 2018.
30. S. A. Elahi, N. Connesson, G. Chagnon, and Y. Payan, "In-vivo soft tissues mechanical characterization: volume-based aspiration method validated on silicones," *Experimental Mechanics*, vol. 59, no. 2, pp. 251–261, 2019.
31. K. Kappert, N. Connesson, S. Elahi, S. Boonstra, A. Balm, F. van der Heijden, and Y. Payan, "In-vivo tongue stiffness measured by aspiration: Resting vs general anesthesia," *Journal of biomechanics*, vol. 114, p. 110147,

2021.

32. G. G. Barbarino, M. Jabareen, and E. Mazza, "Experimental and numerical study on the mechanical behavior of the superficial layers of the face," *Skin Research and Technology*, vol. 17, no. 4, pp. 434–444, 2011.
33. D. Sachs, A. Wahlsten, S. Kozerke, G. Restivo, and E. Mazza, "A biphasic multilayer computational model of human skin," *Biomechanics and modeling in mechanobiology*, vol. 20, no. 3, pp. 969–982, 2021.
34. M. A. Nazari, P. Perrier, M. Chabanas, and Y. Payan, "Simulation of dynamic orofacial movements using a constitutive law varying with muscle activation," *Computer methods in biomechanics and biomedical engineering*, vol. 13, no. 4, pp. 469–482, 2010.
35. M. Pensalfini, J. Weickenmeier, M. Rominger, R. Santoprete, O. Distler, and E. Mazza, "Location-specific mechanical response and morphology of facial soft tissues," *Journal of the mechanical behavior of biomedical materials*, vol. 78, pp. 108–115, 2018.
36. A. Mîra, A.-K. Carton, S. Muller, and Y. Payan, "A biomechanical breast model evaluated with respect to mri data collected in three different positions," *Clinical Biomechanics*, vol. 60, pp. 191–199, 2018.
37. E. Mukhina, P.-Y. Rohan, N. Connesson, and Y. Payan, "Calibration of the fat and muscle hyperelastic material parameters for the assessment of the internal tissue deformation in relation to pressure ulcer prevention," *Computer Methods in Biomechanics and Biomedical Engineering*, vol. 23, no. sup1, pp. S197–S199, 2020.
38. M. Bucki, V. Luboz, A. Perrier, E. Champion, B. Diot, N. Vuillerme, and Y. Payan, "Clinical workflow for personalized foot pressure ulcer prevention," *Medical engineering & physics*, vol. 38, no. 9, pp. 845–853, 2016.
39. D. G. W. Douglas M. Bates, *Nonlinear Regression Analysis and Its Applications*. John Wiley & Sons, Inc, 1988.

40. D. W. Marquardt, "An algorithm for least-squares estimation of nonlinear parameters," *Journal of the society for Industrial and Applied Mathematics*, vol. 11, no. 2, pp. 431–441, 1963.
41. G. Aversano, A. Bellemans, Z. Li, A. Coussement, O. Gicquel, and A. Parente, "Application of reduced-order models based on pca & kriging for the development of digital twins of reacting flow applications," *Computers & Chemical Engineering*, vol. 121, pp. 422–441, 2019.
42. T. Aoki, T. Ohashi, T. Matsumoto, and M. Sato, "The pipette aspiration applied to the local stiffness measurement of soft tissues," *Annals of biomedical engineering*, vol. 25, no. 3, pp. 581–587, 1997.
43. B. Müller, J. Elrod, M. Pensalfini, R. Hopf, O. Distler, C. Schiestl, and E. Mazza, "A novel ultra-light suction device for mechanical characterization of skin," *PloS one*, vol. 13, no. 8, p. e0201440, 2018.